Original scientific paper

Wear behaviour and microstructural characteristics of cold sprayed nickel-alumina coatings on boiler steel

Deepak Dhand[1,2,✉], Parlad Kumar[1] and Jasmaninder Singh Grewal[2]

[1]Department of Mechanical Engineering, Punjabi University, Patiala 147002, India
[2]Department of Mechanical and Production Engineering, Guru Nanak Dev Engineering College, Ludhiana 141006, India

Corresponding author: [✉]dmechd@gmail.com

Abstract

There is an excessive material loss in steel components due to sliding wear in different industrial applications. The SS 316 steel is extensively used in the power generation industry for boilers, induction fans, ducts, etc., and counter-high sliding wear. The studies have shown that protective coatings deposited by thermal spray methods successfully control the wear and enhance the service life of steels. In this work, the nickel-alumina coating was deposited on SS 316 by cold spray technique to understand the effectiveness of coatings in resisting wear. The wear behavior of coatings was analyzed by conducting the wear test on a pin-on-disc apparatus at different loads, i.e., 30, 40 and 50 N keeping the speed constant. The wear trends and variation in friction coefficient due to wear were observed. The mechanical and microstructural characterization was done by FE-SEM/EDS and XRD techniques. The coatings were found effective in resisting the wear on SS 316 steel. The results indicate that the wear rate of coatings increased with an increase in normal load.

Keywords

Cermet coatings; cold spray; sliding wear; pin-on-disk testing; tribology; morphology

Introduction

The SS 316 steel grade is extensively used in pipelines, transfer ducts, shafts, bearings, and other dynamic and static structures of the power plant, petroleum, refinery, and automotive industry [1–3]. It undergoes mild to severe wear effects, both under room and high-temperature conditions. In order to protect it from degradation and enhance its service life, various surface modification techniques such as weld overlays, heat treatments, physical vapor deposition (PVD), chemical vapor deposition (CVD), electroless plating, thermal spray deposition, *etc*., were found useful [4–6]. The thermal spray deposition techniques such as electric arc spray, plasma spray, detonation spray, high-velocity oxygen fuel (HVOF) spray, and cold spray were found highly effective in resisting wear [7]. The thermal spray methods use chemical or electrical energy to melt the feedstock and spray it on the

metal surface at high velocities ranging between 800-1200 m/s. After striking the metal surface, the molten droplets spread out and solidify to provide the protective layer on the steel surface [8].

The recent addition to the thermal spray family is the cold spray (CS) technique. It is one of the advanced methods which can overcome the problems associated with conventional techniques. In this technique, the coating powder is not melted or partially melted and is sprayed at room temperature under controlled conditions on the metal surface. The main advantage of using this technique is that negligible or no oxidation of the feedstock particles takes place during the spray of protective coatings [9,10]. Secondly, due to high spray velocity, *i.e.,* above 800 m/s, the coatings exhibited high density, deposition rate, and lamellar microstructure. It has also proved its compatibility with a wide variety of feedstock materials, *i.e.,* metals, alloys, and ceramics, in the pure or composite form. Koivuluoto *et al*. [11] used the cold spray technique to understand and compare the microstructural and mechanical properties of Cu, Ni, and Zn-based coatings. Gao *et al*. [12] studied the influence of powder morphology on the deposition of coatings by the cold spray technique. The researchers revealed that the CS technique exhibited high deposition efficiency when loosely bound cermet feedstock was used. Therefore, this technique is widely investigated by researchers [13,14].

The nickel metal is known for its stability, corrosion, and wear resistance in room and high-temperature applications. Khan *et. al.* [15] studied the sliding wear behavior of nickel-based super-alloys on nickel-chromium-based cermet coatings by using pin-on-disc apparatus. It was found that the coating helped in resisting the wear. Similar types of research were also done by other researchers [16,17]. Researchers have also explored its tribological behavior in the form of cermet. The studies have shown that cermet coatings helped to enhance the wear resistance performance of coatings. The hard ceramics used in protective coatings are usually carbides or oxides of tungsten, chromium, or aluminum. The metal matrix composites exhibit high strength and improved wear resistance over the base metals. Previous studies have shown that the method of deposition plays a key role in governing the wear resistance behavior of metal-matrix composite coatings [18–21]. However, most of the studies reported the metal matrix composites based on tungsten-carbide or chromium-carbide, while the limited literature is available related to nickel-based cermet coatings.

In the present investigation, the cold spray technique is used to deposit the nickel-alumina cermet coating on SS 316. This article will help the researchers to understand the tribological behavior and mechanisms of cermet coatings deposited by the cold spray technique. The focus of this work is to study the microstructural characteristics and analyze the wear behavior of the coatings in increasing load conditions at room temperature during testing on the pin-on-disc test rig. The coated and worn-out surfaces are analyzed by using the FE-SEM (Field emission scanning electron microscope) and XRD (X-ray diffraction) techniques.

Experimental

Deposition of coating

The SS 316 steel was used for the coating deposition. The chemical composition of (stainless steel) SS 316 is shown in Table 1. The pin samples having size ϕ 6 ×30 mm were prepared from the bar. Before applying coatings, the samples were polished with emery papers of grades 180, 400, 800, and 1200 and grit blasted. The electrolytically prepared nickel-alumina (Ni-Al$_2$O$_3$) powder (K-32) was supplied and sprayed by M/s MECPL, Jodhpur, with the cold spray technique using standard spray parameters. The cold spray equipment used the air as a process gas at the pressure of 65 μPa. The feedstock powder was fed at the rate of 30 g min^{-1} through the spray gun having a temperature range of 200-600 °C, keeping the spray distance of 10-12 mm from the substrate.

Table 1. *The chemical composition of SS 316.*

Element	C	Cr	Ni	Mn	Si	Cu	Mo	P	S	Fe
Content, wt.%	0.7	17.0	11.0	1.12	0.7	0.1	2.0	0.02	0.03	balance

Characterization

The surface morphology of coating powder and coatings was studied with FE-SEM (JEOL7610F) and the elemental composition was found by EDAX attached with it. The phases developed during the deposition of the coatings were determined after analyzing the patterns of the X-ray diffraction (XRD) diffractometer with Bruker D8 using Cu radiations. The porosity of coated samples was measured with the optical microscope, XJL-17. The surface roughness of coatings was determined with Mitutoyo, a surface roughness tester, in terms of R_a values. The average micro-hardness coated samples were determined using the Vickers micro-hardness tester as per ASTM standards. The average values were calculated after taking an average of 10 readings at different points. Before analyzing the microstructural characteristics, the samples were polished and cleaned properly with acetone to remove any unwanted particles present on the coated surface.

Wear testing

The pin-shaped samples were tested for wear test on a pin-on-disk test rig (DUCOM) to determine their wear and friction behavior. The CS samples were slid against the hardened EN31 steel disc on the apparatus at room temperature and dry conditions. The counter steel disc used in the apparatus (EN31 grade) had a hardness value of 550 HV. A track radius of 60 mm was selected. The pin was fixed into a steady pin holder and pressed against the counter disc with a normal load of magnitude 30, 40, and 50 N, individually keeping the rotating speed of the counter disc constant at 1 m/s. The wear rate and coefficient were measured online with the interface data analyzing software for every test cycle. The software evaluated wear in pin samples in terms of loss of pin length (in micrometers) with the increase in sliding distance. The wear rate of every worn-out sample was calculated by measuring the area of the wear track, which was an average of five measurements, and then the wear volume was calculated. The schematic view indicates various elements of the pin-on-disc apparatus, as shown in Figure 1.
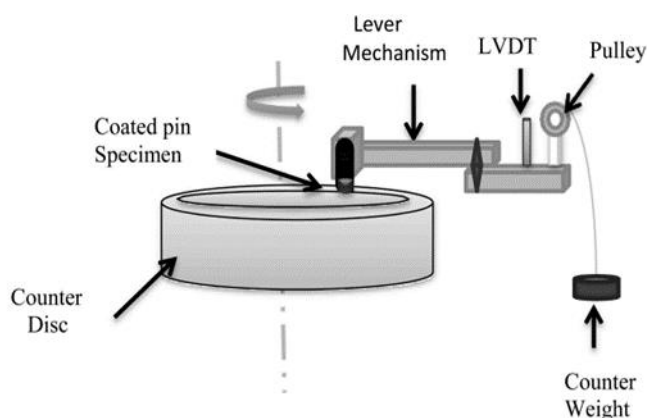

Figure 1. *Schematic view of various elements of the pin-on-disc tribometer*

Results and discussion

Microstructural characterization of powder and coatings

The electrolytically prepared nickel-alumina powder used in the deposition of coatings was provided by the manufacturers of the cold spray equipment. The customized powder was prepared

specially to use in the low-pressure cold spray equipment. As the SEM image in Figure 2 represents, the particle morphology of the powder is highly irregular. The alumina particles have rigid, brittle, and blocky structures, whereas the nickel particles have globular and fibrous structures. The particles of both constituents were randomly distributed in an undefined pattern. The average size range of alumina particles was found in 25-30 µm, whereas for nickel particles, it was between 35-60 µm.
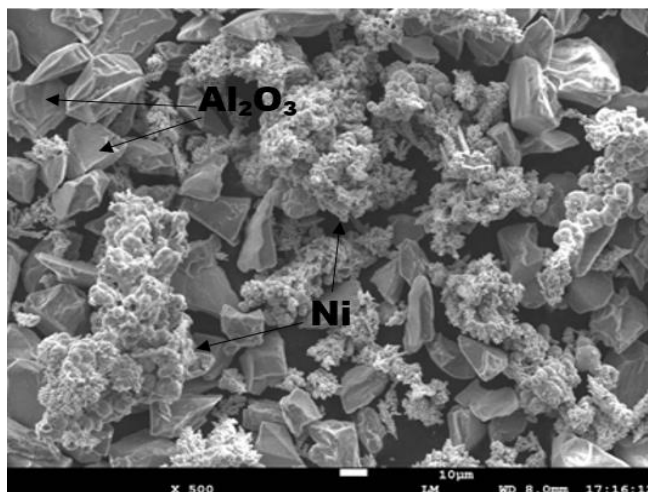

Figure 2. SEM image of nickel-alumina powder

During the visual inspection of the as-sprayed coatings, it was found to have a smooth, hard, and lamellar structure in grey color. On observing the same samples with SEM shown in Figure 3, it was found that the coating has a thick splat microstructure. The nickel-alumina particles were completely fused into each other. The presence of small pores was also noticed without any indication of a major crack on the surface of coatings. However, the porosity of the coatings was in the range of 2-3 %. In Figure 3, the irregular bright particles were revealed as nickel elements, whereas the alumina particles were revealed as dark shaded elements. The average value of coating thickness was found at 629 µm and the average micro-hardness of coatings was 171 HV. The surface roughness of the coatings was found at 6.62 µm (R_a value).
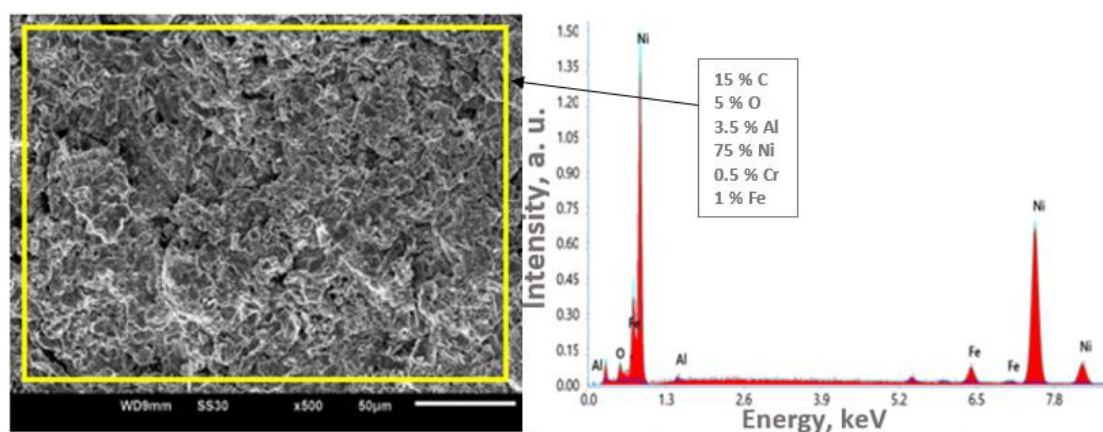

Figure 3. SEM image and EDS analysis of the coated sample

The cross-sectional microstructure of the cold sprayed nickel-alumina coating on steel substrate in Figure 4 represents the dense and layered morphology. The coating was found intact with the substrate surface throughout the length of the sample. The presence of voids was also noticed due to the formation of splats of coating material during the deposition process.
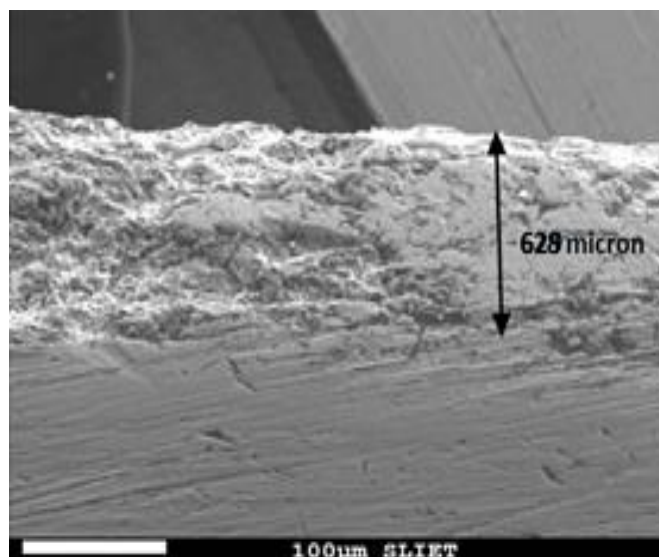
Figure 4. *Cross-sectional SEM image of the coated sample*

Figure 5 represents the XRD pattern of the as-spray coated sample. The XRD graph reveals the amorphous behavior of coating. The analysis of the XRD pattern indicated the presence of major phases consisting of Ni, Ni_3Al, and Al_2O_3. The nickel-aluminide (Ni_3Al) formed during the process possesses good stability at high temperatures. The weak phases consisting of NiO and NiAl were found present in a negligible amount in the coating microstructure.
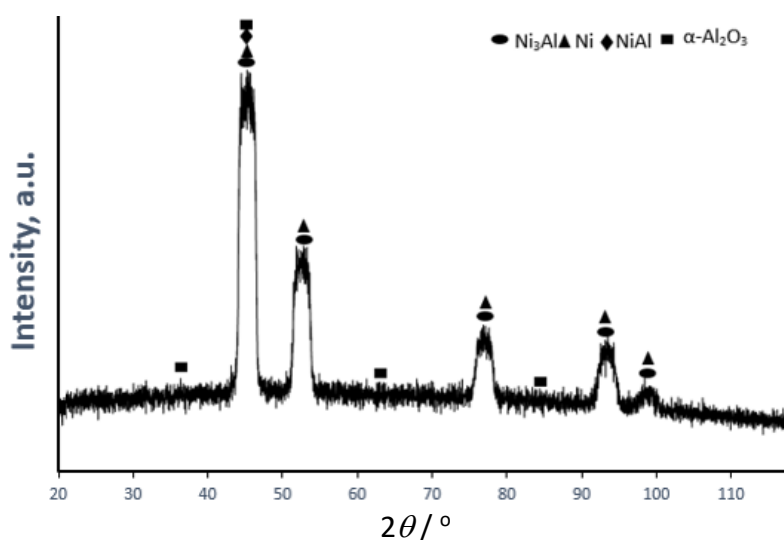

Figure 5. *XRD pattern of the as-sprayed sample.*

Wear trends of coatings

Figure 6a-6c shows the typical variation of wear of nickel-alumina coated pin sample with the increase in the sliding distance during testing on pin-on-disc apparatus. As indicated in Figure 6a, the loss of pin length due to wear raised for approx. 400 m of sliding distance and then fall suddenly. This wear behavior of coatings was due to pulling out of coating particles at the initial testing stage at 30 N normal load. It was found that during the whole test cycle, negligible loss of length of sample was recorded. For the same test cycle, the variation of the coefficient of friction (COF) is represented in Figure 6d. It shows that the COF reflected minimal disturbance throughout the cycle representing the increasing trend starting from 0.29 (at 11 m of SD) value to 0.51 (at 5399 m of SD). Similar trends were also revealed by several researchers [21–23]. Similarly, as shown in Figure 6b, when a normal load of 40 N is applied, the loss of pin length represented the abrupt changes during the initial 700

m of sliding distance. After 700 m, the wear behaviour of the sample represented a regular pattern of material removal. A similar trend can be observed with the COF plot given in Figure 6e. It is also found from the plot that the range of COF decreased as compared to that which is represented during testing at 30 N load. Figure 6c shows the loss of length in the coated sample at 50 N of normal load. The wear trend represented by the plot is very uncertain, up to 3700 m of sliding distance. Above this, there was an abrupt rise in length loss of pin sample and showed highly increasing-decreasing trends. These variations in wear trends can also be further co-related with the trends of COF shown in Figure 6f. The reason behind this wear behaviour and COF is discussed in detail with SEM images in the next section.
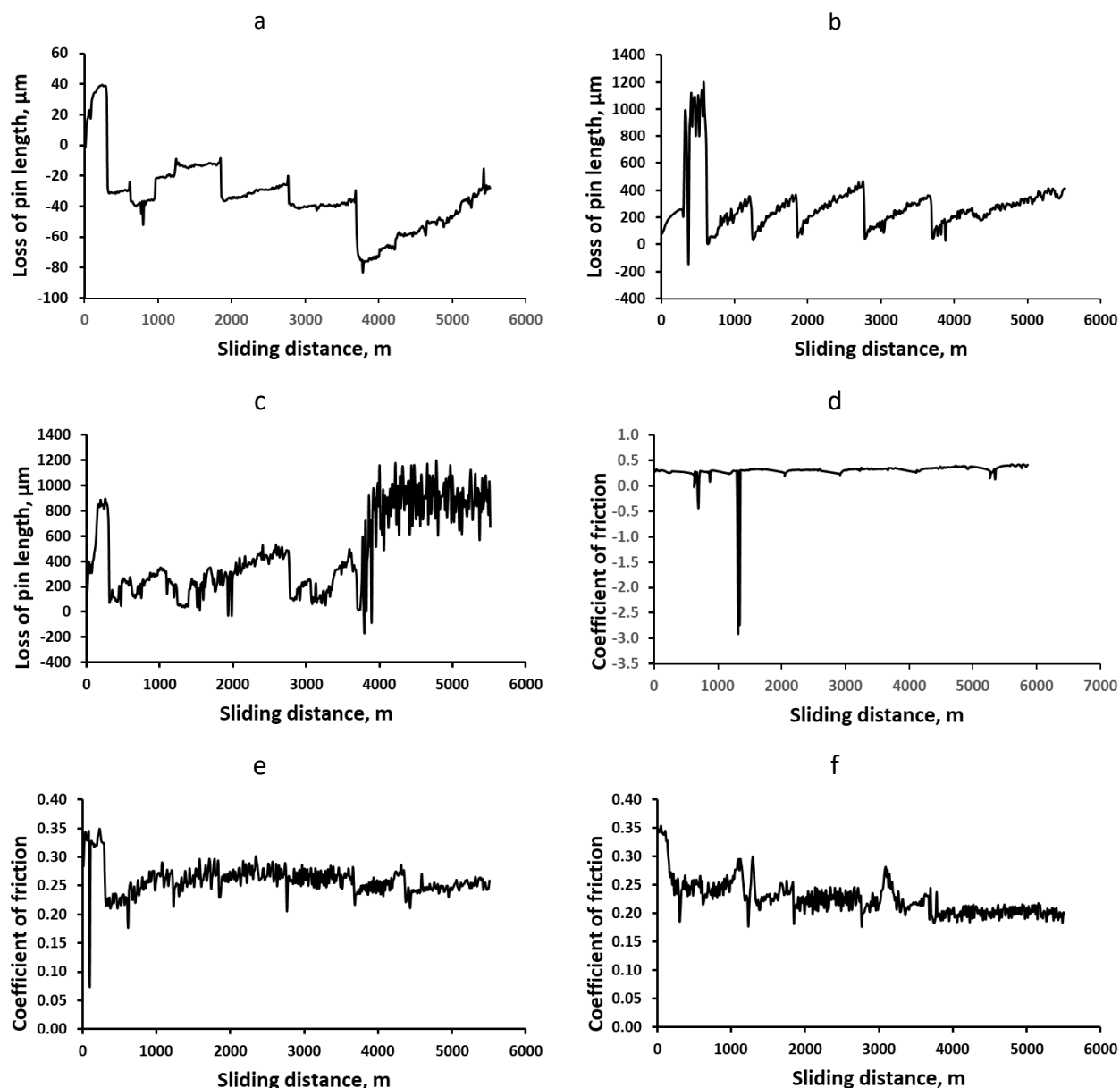

Figure 6. *Wear trend of pin sample at a normal load of (a) 30 N, (b) 40 N, (c) 50 N and the variation of COF at a normal load of (d) 30 N, (e) 40 N, (f) 50 N*

The wear trend shown by the as-spray coated pin samples and the variation of COF during each test cycle at different normal loads are summarized and compared with the bare steel in Figures 7a and 7b, respectively.

As discussed above, the wear rate of as-sprayed coated samples was almost negligible at 30 N load. With the increase in normal load, *i.e.,* at 40 N and 50 N, the wear rate of the coatings increase, but these trends follow the opposite direction for bare steel. On the other hand, the average value of COF was found highest at 30 N load, both for coated and bare steels. As the graph in Figure 7b represents, with the increase in normal load values, the COF between the rotating counter plate and the tip of the pin sample decreased.
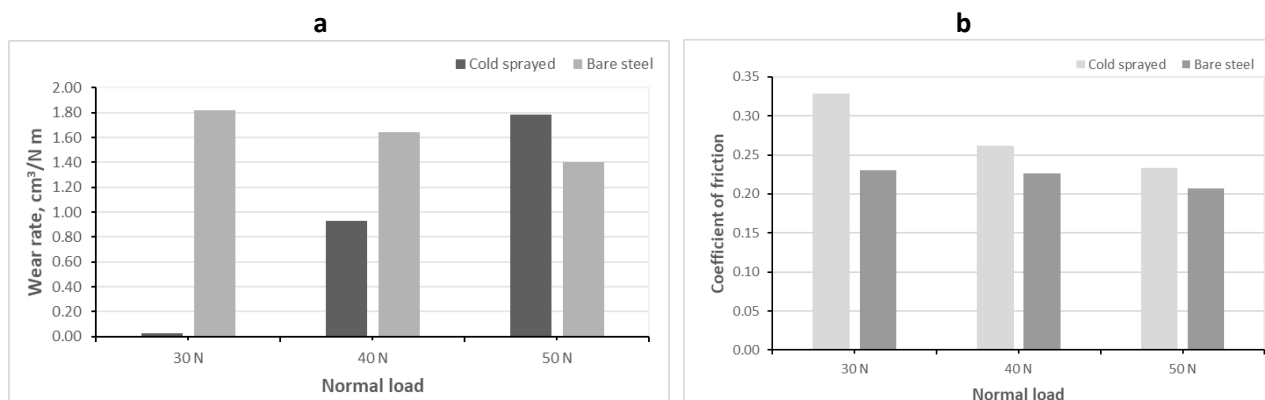

Figure 7. *(a) Wear rate vs. load and (b) coefficient of friction (COF) vs. load*

Analysis of worn-out surfaces

The SEM image in Figure 8a represents the surface morphology of the worn-out sample tested at 30 N of normal load and 1 m/s sliding speed. As indicated in Figure 8a, during the initial stage of the low loading condition, the coating particles were pulled out after sliding to a certain distance by the coated tip of the pin sample. Initially, these particles cause three-body abrasion between the rotating counter plate and the coated surface of the pin sample exposed to the counter plate. This rise in wear was also justified by Figures 6a and 6d. After this, some of these pull-out particles get adjusted in the pores of coatings, while others draw wear tracks on the surface of the coating under test. This stabilizes the varying trends in wear and COF graphs, represented at the tails of the plot (above 4000 m).

Figure 8b indicates the ploughing by the wear particles at moderate loads, *i.e.,* 40 N. The SEM image also exhibits the partial delamination of the coating layer along with particle removal. The represented image, however, shows a relatively smooth and less uneven surface compared with the surface morphology represented by the worn-out sample at 30 N. On relating the SEM image shown in Figure 8b with the wear trends in Figure 6b, represented as sharp declining trends at certain intervals. This wear behavior of coatings was due to the peeling off wear mechanism of the coated layer after sliding through a certain distance against the rotating disc.

The SEM image shown in Figure 8c indicates the presence of wear debris and peeling off the coatings when the normal load is increased to 50 N during the wear testing. The delamination of coatings was found to be a dominant wear mechanism along with the presence of wear debris at high loads. Due to this wear behavior, a high wear rate and low COF were observed in Figures 6c and 6f. Moreover, the formation of uneven oxide and carbide films on the coating surface during wear at high load was also observed in the SEM image. The elemental composition of one of the films is represented in the EDS analysis shown in Figure 8c. These films were brittle in nature which later got converted into wear debris and found responsible for ploughing and micro-cracking the coating layers.
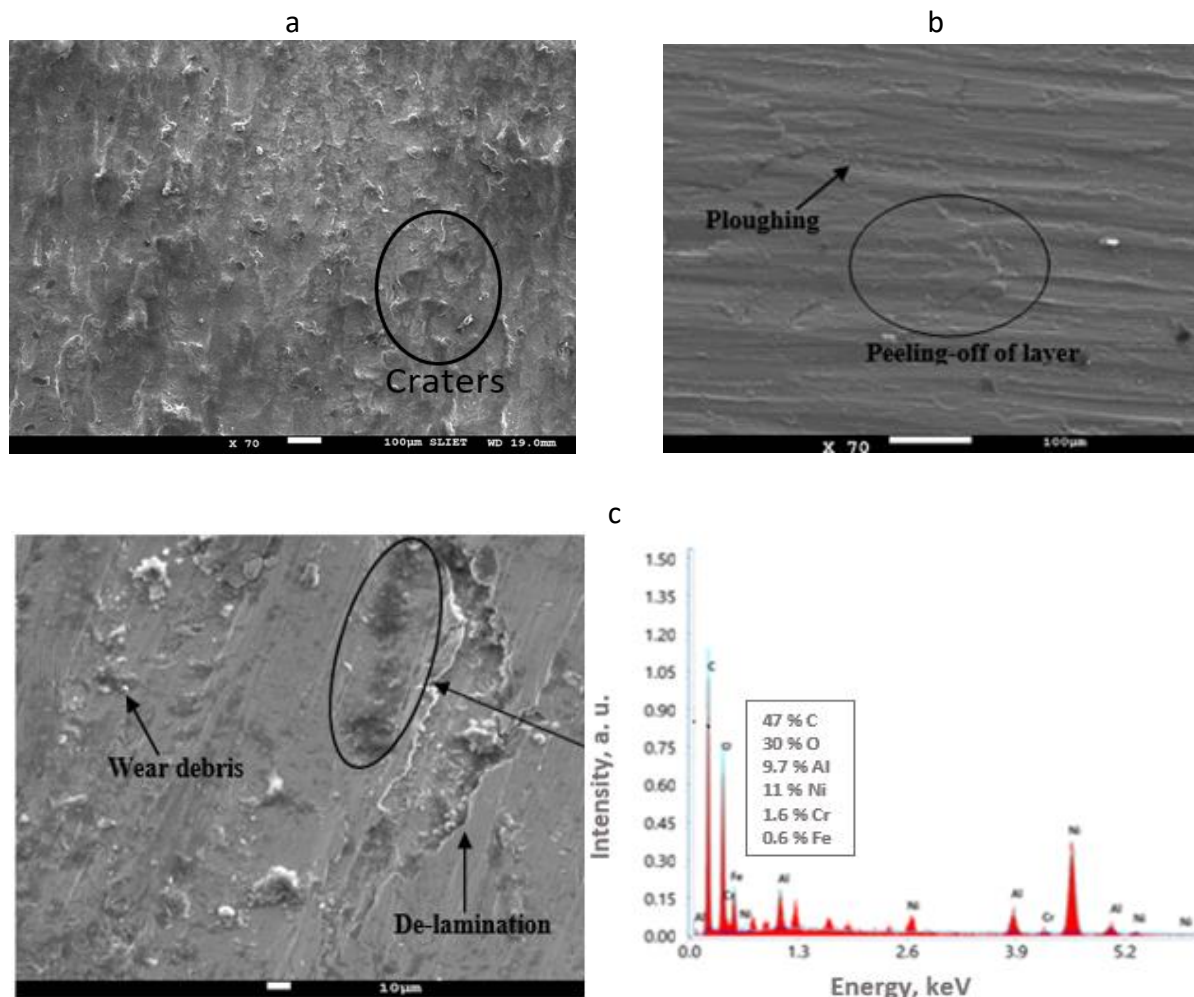
Figure 8. *SEM images of the worn-out surface of the as-sprayed sample at (a) 30 N, (b) 40 N, (c) 50 N, along with EDS of the image*

Conclusions

The cold sprayed nickel-alumina coatings successfully resisted the sliding wear at low loads, but its performance decreased with the increase in load. This was due to the bulk removal of coating material at high normal loads. The coefficient of friction value between the rotating counter plate and the stationary tip of the coated sample decreased with the increase in normal load due to flattened coated layers at high loads. The delamination of coatings, micro-cracks, formation of uneven films of oxide-carbides, and wear debris were dominant wear mechanisms at high normal loads. Whereas wear due to pulled-out coating particles, formations of pits, and adhesion of wear particles with the coated surface were the major wear mechanisms at low loading conditions, as observed with the FE-SEM technique.

References

[1] S. Kumar, M. Kumar, A. Handa, *Engineering Failure Analysis* **94** (2018) 379-395. http://doi.org/10.1016/j.engfailanal.2018.08.004
[2] A. V. Levy, *Wear* **138(1–2)** (1990) 111-123. http://doi.org/10.1016/0043-1648(90)90171-6
[3] E. Raask, *Wear* **13(4–5)** (1969) 301-315. http://doi.org/10.1016/0043-1648(69)90252-X

[4] D. Rezakhani, *Anti-Corrosion Methods and Materials* **54(4)** (2007) 237-243. http://doi.org/10.1108/000355907107-2384

[5] J. Mehta, V. K. Mittal, P. Gupta, *Journal of Applied Science and Engineering* **20(4)** (2017) 445-452. http://doi.org/10.6180/jase.2017.20.4.05

[6] R. J. K. Wood, J. A. Wharton, *11-Coatings for tribocorrosion protection,* in *Tribocorrosion of Passive Metals and Coatings,* D. Landolt, S. Mischler, Ed(s)., Woodhead Publisher, UK, 2011 296-333. http://doi.org/10.1533/9780857093738.2.296

[7] D. Dhand, P. Kumar, J. S. Grewal, *Corrosion Reviews* **39(3)** (2021) 243-268. https://doi.org/10.1515/corrrev-2020-0043

[8] L. Pawlowski, *The Science and Engineering of Thermal Spray Coatings,* Second Edition, Published by John Wiley & Sons Ltd, UK, 2008 1-626. http://doi.org/10.1002/9780470754085

[9] H. Singh, T. S. Sidhu, S. B. S. Kalsi, *Frattura Ed Integrità Strutturale* **22** (2012) 69-84. http://doi.org/10.3221/IGF-ESIS.22.08

[10] M. F. Smith, *3-Comparing cold spray with thermal spray coating technologies*, in *The Cold Spray Materials Deposition Process: Fundamentals and Applications*, V. K. Champagne, Ed., Woodhead Publisher, UK, 2007 43-61. http://doi.org/10.1533/9781845693787.1.43

[11] H. Koivuluoto, J. Lagerbom, M. Kylmälahti, P. Vuoristo, *Journal of Thermal Spray Technology* **17** (2008) 721-727. http://doi.org/10.1007/s11666-008-9245-6

[12] X. Guo, G. Zhang, W. Li, Y. Gao, H. Liao, C. Coddet, *Applied Surface Science* **255(6)** (2009) 3822-3828. http://doi.org/10.1016/j.apsusc.2008.10.041

[13] M. Ashokkumar, D. Thirumalaikumarasamy, P. Thirumal, R. Barathiraja, *Materials Today: Proceedings* **46(17)** (2021) 7581-7587. http://doi.org/10.1016/j.matpr.2021.01.664

[14] B. V. Padmini, M. Mathapati, H. B. Niranjan, P. Sampathkumaran, S. Seetharamu, M. R. Ramesh, N. Mohan, *Materials Today: Proceedings* **27(3)** (2019) 1951–1958. http://doi.org/10.1016/j.matpr.2019.09.025

[15] M. A. Khan, S. Sundarrajan, M. Duraiselvam, S. Natarajan, A. Senthil, A. S. Kumar, *Surface Engineering* **33(1)** (2017) 35-41. http://doi.org/10.1179/1743294415Y.0000000087

[16] V. Higuera Hidalgo, J. Belzunce Varela, A. Carriles Menéndez, S. Poveda Martínez, *Wear* **247(2)** (2001) 214-222. http://doi.org/10.1016/S0043-1648(00)00540-8

[17] V. Higuera Hidalgo, J. Belzunce Varela, J. Martínez de la Calle, A. Carriles Menéndez, *Surface Engineering* **16(2)** (2000) 137-142. http://doi.org/10.1179/026708400101517035

[18] D. Aussavy, S. Costil, O. El Kedim, G. Montavon, A. F. Bonnot, *Journal of Thermal Spray Technology* **23(1–2)** (2014) 190–196. http://doi.org/10.1007/s11666-013-9999-3

[19] S. S. Chatha, H. S. Sidhu, B. S. Sidhu, *Surface and Coatings Technology* **206(19–20)** (2012) 3839-3850. http://doi.org/10.1016/j.surfcoat.2012.01.060

[20] T. Peat, A. Galloway, A. Toumpis, P. McNutt, N. Iqbal, *Applied Surface Science* **396** (2017) 1635-1648. http://doi.org/10.1016/j.apsusc.2016.10.156

[21] D. Dhand, J.S. Grewal, P. Kumar, *Surface Topology: Metrology and Properties* **9(4)** (2021) 045056. https://doi.org/10.1088/2051-672X/ac4402

[22] V. N. V. Munagala, S. Bessette, R. Gauvin, R. R. Chromik, *Wear* **450–451** (2020) 203268. http://doi.org/10.1016/j.wear.2020.203268

[23] J. M. Shockley, S. Descartes, E. Irissou, J.-G. Legoux, R. R. Chromik, *Tribology Letters* **54(2)** (2014) 191-206. http://doi.org/10.1007/s11249-014-0326-z